THE JOURNAL OF PHYSICAL CHEMISTRY B

Article

pubs.acs.org/JPCB

Enhanced Architecture of Lipid-Carbon Nanotubes as Langmuir–Blodgett Films to Investigate the Enzyme Activity of Phospholipases from Snake Venom

Luciano Caseli,*[,†] Vera L. B. Tiburcio,[‡] Frey F. R. Vargas,[§] Sérgio Marangoni,[§] and José R. Siqueira, Jr.*[,‡]

[†]Federal University of São Paulo (UNIFESP), Diadema, São Paulo (SP), 09972-27, Brazil

[‡]Federal University of the Triângulo Mineiro (UFTM), Uberaba, Minas Gerais (MG), 38025-180, Brazil

[§]State University of Campinas (UNICAMP), Campinas, São Paulo (SP), 13083-970, Brazil

ABSTRACT: The immobilization of biomolecules in films with a controlled architecture permits the access of information on the molecular interactions, not only between film components, but also between the film and substances in the external environment. In this study, we investigated the immobilization of the phospholipase A_2 from snake venoms (4-nitro-3-(octanoyloxy)benzoic acid, OBZ) in solid supports as a Langmuir–Blodgett (LB) film, followed by incorporation of carbon nanotubes (CNTs). The hybrid film was characterized by infrared spectroscopy and the interactions with its catalytic substrate were investigated. The presence of CNTs leads to a structure with an adequate environment to preserve the enzyme properties, leading to an optimum catalytic activity. This enhanced architecture was exploited in terms of vibrational spectroscopy, which indicated changes in the secondary structure of the enzyme upon contact with the catalytic substrate.

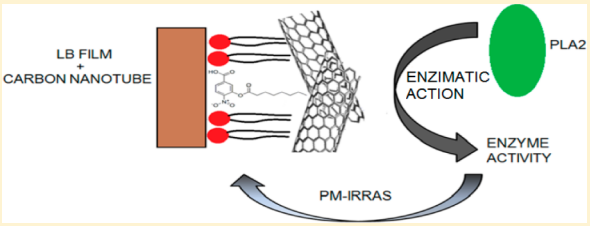

1. INTRODUCTION

The adequate manipulation of biomolecules in ultrathin films has been one of the keys in biotechnology to develop hybrid materials with enhanced properties, which may be employed in biomedical applications, such as drug delivery and biosensors.[1−3] Particularly, there has been growing interest in snake venom components responsible for biological effects, such as neurotoxic, myotoxic, cardiotoxic, anticoagulant, hypotensive, hemolytic, platelet aggregation inhibiting, bactericidal, hemolysis, and pro-inflammatory activities.[4,5]

The snake venom is a complex mixture that contains a variety of proteic components (oxidoreductases, hydrolases, proteases, glycosidases, and lypases) and nonproteic ones, as inorganic (magnesium, calcium, and zinc ions) and organic (amino acids, lipids, carbohydrates, and nucleic acids). In particular, the phospholipase A_2 (PLA2) is a thermostable enzyme able to act on nonaqueous systems and on the surface of nanoparticles and lipid monolayers.[6] PLA2 belongs to a family of lipases that have low catalytic activity.[7] These catalytically active enzymes cleave the sn-2 acyl bond of glycerophospholipids, releasing free fatty acids and lysophospholipids.[8]

In this context, comprehension of how PLA2 acts is important not only for the detection of traces of venom in samples, but also for understanding the molecular aspects involved in the catalytic reactions. Therefore, developing strategies able to investigate the involved interactions at the molecular level is of interest. As many of these interactions occur on hydrophobic surfaces, the use of ultrathin films for molecular investigations is adequate.

The Langmuir–Blodgett (LB) technique is an excellent tool to assemble ultrathin films.[9] For that, a monomolecular film is first prepared at the air–water interface. Such monolayers are usually formed with amphiphilic and water insoluble materials, and the surface packing can be regulated by the action of movable barriers that laterally compress the interface. If compressed up to a given surface pressure, the monolayer can be transferred from the liquid interface to solid supports forming the so-called Langmuir–Blodgett films. The number of layers (and, consequently, the thickness of the film) can be controlled by successive passages of the solid support through the interface. These films are molecularly ordered and have been employed for studies of sensors,[10−12] electronic devices,[13−15] bioinspired materials,[16−18] and biomembranes models.[19−21]

The employment of biomolecules with molecular recognizing properties in LB films has been recently reported.[22−24] The use of the pair enzyme/substrate has become one of the most popular strategies to investigate the viability of constructing biosensors by using the LB technique. In addition, some substances can be further incorporated to enhance the optical or electrical signal of interest.

Particularly, it has been reported that carbon nanotubes (CNTs) may improve charge transfer. They are also capable of changing the conformation of molecules incorporated in hybrid films.[25−30] In a previous work, CNTs were incorporated in a

Received: July 31, 2012
Revised: October 25, 2012
Published: October 29, 2012

DMPA-urease hybrid LB film, modifying significantly the organization of the compounds adsorbed on the solid support and creating an appropriate environment to preserve the enzymatic activity of enzyme. Furthermore, the film presented enhanced performance and sensitivity to detect urea, which may enable the future construction of urea biosensors.[12] In terms of biocompatibility, CNTs are advantageous regarding the fact that they can allow the immobilization of biomolecules with their biological activity preserved. This may provide materials with electronic properties that allow direct charge transfer from proteins to electrode surfaces.[31−37] Moreover, hybrid films based on CNTs lead to the formation of porous ultrathin structures with large surface areas that may contribute to a better electrode−electrolyte interface. Such film morphology is important for the development of sensing units with enhanced properties.[10−12,27,28]

In this paper, we present for the first time the introduction of CNTs in lipid hybrid Langmuir−Blodgett films and their effect on the enzyme activity of phospholipases from snake venoms. The influence of CNT incorporation over the surface chemistry of the films and their interactions are discussed, as well as the consequences and advantages in terms of enzyme activity preservation.

2. EXPERIMENTAL SECTION

2.1. PLA2 Purification. The phospholipase A_2, denominated CDC-10, were isolated from *Crotalus durissus cumanensis* venom and purified according to the protocol reported by Romero-Vargas et al.[38] The chemicals used in this purification were of analytical grade.

2.2. Materials. Stearic acid (HSt), carbon nanotube, single-walled, polyaminobenzene sulfonic acid functionalized, and 4-nitro-3-(octanoyloxy)benzoic acid were purchased from Sigma-Aldrich. Water was supplied by a Milli-Q system (resistivity = 18.2 MΩ cm at 23 °C and pH 6.3). All other reagents were of the highest purity commercially available and were also purchased from Sigma-Aldrich.

2.3. Langmuir Monolayer Preparation and Characterization. Langmuir monolayers were prepared on a mini-KSV Langmuir trough (system 2, total volume of 220 mL), equipped with a Wilhelmy plate made of a filter paper. Langmuir monolayers of stearic acid were obtained by spreading its solution in chloroform (Sigma, high-performance liquid chromatography (HPLC) grade) on the surface of pure water.

Surface pressure−area (π−A) isotherms were obtained with a monolayer compression rate of 0.5 $Å^2$ $molecule^{-1}$ min^{-1}, with the subphase at temperature of 23 ± 1 °C. Stearic acid monolayer was compressed about 20 min after solvent evaporation. 3,4-Octanolxy benzoic−stearic acid (1:99 molar rate) mixed monolayers were obtained by premixing both components in chloroform. Polarization−modulation infrared reflection absorption spectroscopy (PM-IRRAS) measurements were carried out with a KSV PMI 550 instrument (KSV Instrument, Ltd., Helsinki, Finland). The Langmuir trough was set up so that the light beam reached the monolayer at a fixed incidence angle of 75°. The incoming light was continuously modulated between *s* and *p* polarization at a high frequency, allowing simultaneous measurement of the spectra for the two polarizations. The difference between the spectra provided surface specific information and the sum of the reference spectrum. With the simultaneous measurements, the effect of the water vapor is largely reduced. The resolution of the spectra was 8 cm^{-1}.

2.4. Langmuir−Blodgett Films. The transfer of the mixed monolayers onto solid supports (quartz or quartz crystal microbalance plates) was performed at a surface pressure of 30 mN m^{-1}. The monolayer was kept at this pressure for 20 min to guarantee stability, after which the solid support, already dipped in the subphase, was removed from the subphase. The dipping speed was 2.0 mm min^{-1}, and the transfer ratio (always close to 1.0) served as a first parameter of quality. Additionally, the LB films were inserted in suspensions of CNTs (0.5 mg mL^{-1} in water) for 10 min and washed with water.

The formation of hybrid films onto the solid support was confirmed with PM-IRRAS and nanogravimetry analyses with a quartz crystal microbalance (QCM, Stanford Research Systems, Inc.) to evaluate the mass transferred to the solid support. For PM-IRRAS and for the determination of the enzyme activity, quartz as a solid support was employed. AT-cut quartz crystals, coated with Au (Stanford Research Systems, Inc.) with a fundamental frequency of about 5 MHz, was utilized for QCM measurements.

2.5. Enzyme Activity. The PLA2 activity determination was carried out three times according to the method previously reported in refs 39 and 40 and adapted to a microplate.[41] The assay mixture contains the following buffer: 10 mM Tris-HCl, 10 mM $CaCl_2$, and 100 mM NaCl, pH 8. After the addition of the LB film in a solution containing PLA2, the mixture was incubated at 37 °C for 40 min and the absorbance at 425 nm was monitored over time.

3. RESULTS AND DISCUSSION

The enzyme catalytic substrate, 4-nitro-3-(octanoyloxy)benzoic acid (OBZ), with low solubility in water, was incorporated in the spreading solution with HSt. When OBZ is spread alone on the aqueous surface, the compression of the monolayer does not cause a significant increase in surface pressure due to its relative low solubility in water and due to its aggregation at the aqueous surface. This is not only associated with the low surface activity of the compound, but also to its poor ability to spread on the air−water interface. However, when mixed with another compound with higher spreading capacity, OBZ can be easily cospread, as denoted in the surface pressure−area isotherm shown in Figure 1. The curves indicate that OBZ affects the HSt monolayer causing the isotherm to shift to higher molecular areas. Determining the molecular area per

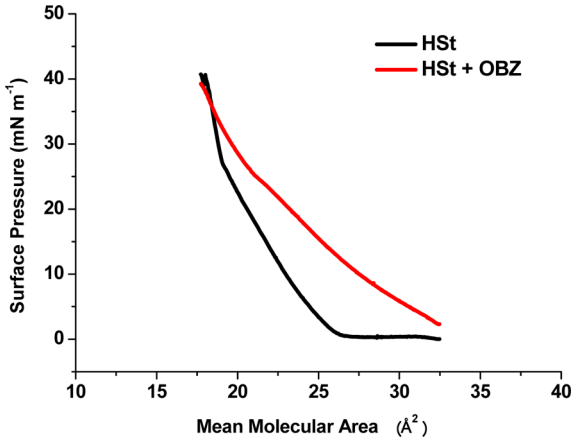

Figure 1. Surface pressure−area isotherms for stearic acid (HSt) monolayers and pure and mixed with OBZ (1% in mol), as indicated in the inset.

dx.doi.org/10.1021/jp307585k | J. Phys. Chem. B 2012, 116, 13424−13429

OBZ is not possible because of its partial solubility in the aqueous subphase. This is also the reason why the surface pressure variation is shown as a function of HSt molecular area. This shift in the curve is attributed to the incorporation of OBZ at the interface, which not only expands the monolayer, but also increases the film surface compressibility. The reciprocal of the surface compressibility, denoted here as in-plane elasticity,[42] is calculated by the expression: $E = -A(\partial\pi/\partial A)_T$, where π is the surface pressure, T is the absolute temperature, and A is the molecular area. The elasticity value, taken at the surface pressure of 20 mN m^{-1}, changes from 205 mN m^{-1}, for pure HSt, to 87 mN m^{-1}, for the mixed monolayer. This indicates a disruption of the ability of the film to pack densely, affecting the monolayer condensation. Then, a lower value of in-plane elasticity is associated to higher monolayer fluidities.

At 34 mN m^{-1}, the values of molecular area are practically the same for both monolayers. Although this could be associated to the complete expelling of the more aqueous soluble component (i.e., OBZ) toward the aqueous subphase, it is likely that OBZ is still affecting the monolayer since the elasticity continues to be lower for the mixed monolayer than for the pure HSt monolayer. It is not unlikely that the more aqueous soluble component remains below the polar heads of the lipid forming a kind of "subsurface". Although this configuration does not affect the molecular area in a given surface pressure, the subsurface formation can alter some rheological properties of the film.

The monolayers were also characterized by PM-IRRAS, as shown in Figure 2. The spectra show the bands for C−H

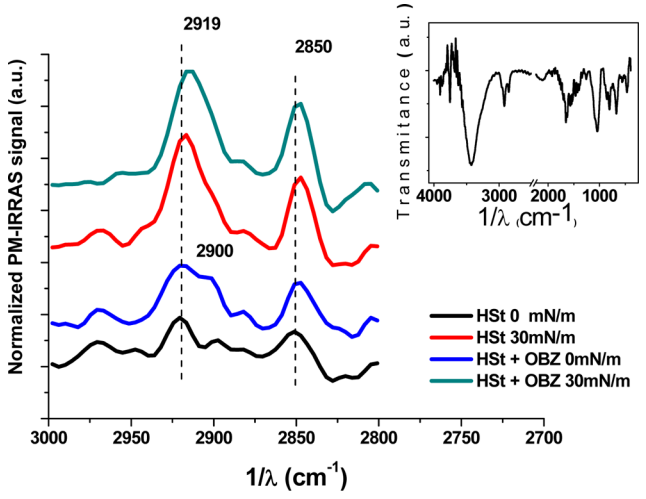

Figure 2. PM-IRRAS spectra for HSt monolayers, pure and mixed with OBZ (1% in mol), as indicated in the inset. The upper inset shows the FTIR spectrum for OBZ in KBr pellets.

stretching in CH_2, attributed mainly to the hydrophobic HSt groups. The band in 2919 cm^{-1} is attributed to asymmetric stretches and in 2951 cm^{-1} to symmetric ones. After introducing OBZ, the asymmetric/symmetric ratio in terms of band intensities decreases, and a band in 2900 cm^{-1}, due to gauche defects in CH_3, appears in the spectra. This ratio changes from 1.7 to 1.4 when the surface pressure of 30 mN m^{-1} is attained. This indicates that OBZ causes a conformational disorder in the monolayer, which corroborates to the hypothesis that OBZ increases the fluidity of the monolayer as previously observed in Figure 1. FTIR in KBr pellets for OBZ is shown in the inset for comparison. One can see that bands for methylene groups (2919 and 2951 cm^{-1}) also appear in the spectrum for OBZ, and this is in agreement with the fact that the presence of OBZ in the monolayer must affect the region of bands presented in Figure 2 for HSt monolayers.

Figure 3 shows the PM-IRRAS spectra for the range of 1000−1800 cm^{-1}, and can be compared to the spectra in the

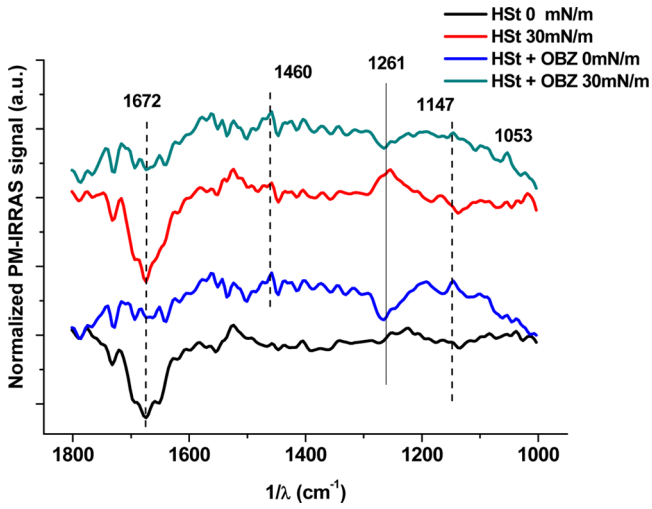

Figure 3. PM-IRRAS spectra for HSt monolayers, pure and mixed with OBZ (1% in mol), as indicated in the inset.

inset of Figure 2. For low surface pressures, the band in 1147 cm^{-1}, attributed to C−O−C antisymmetric stretch in ethers, is visible in the spectrum, confirming the presence of OBZ at the interface, as represented in Figure 4. The FTIR spectrum in KBr pellets also presents a band in this region (~1150 cm^{-1}). At higher surface pressures, this band is less evident, corroborating the initial hypothesis in which OBZ is partially expelled from the monolayer upon compression. Another main change upon substrate incorporation is the inversion of the

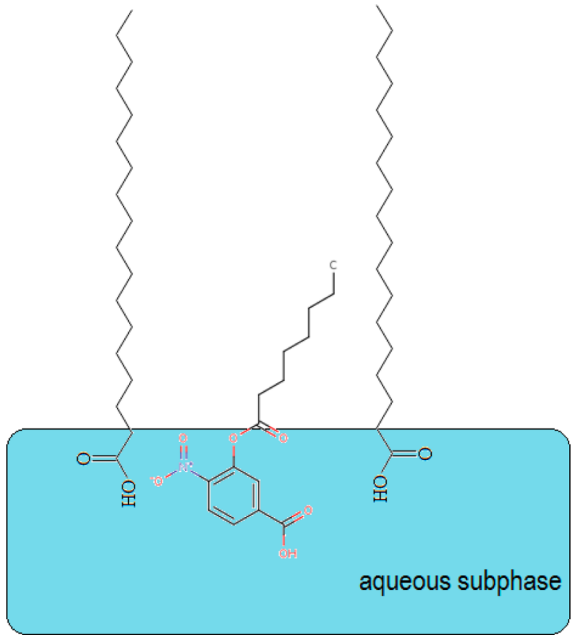

Figure 4. Scheme for the formation of the hybrid HSt-OBZ monolayer.

dx.doi.org/10.1021/jp307585k | J. Phys. Chem. B 2012, 116, 13424−13429

band in 1261 cm^{-1}, which is assigned to a coupled mode of the C−O stretching and the OH in-plane bending vibrations of the *trans*-configuration.[43,44] One can also observe the inverted-to-the-baseline band for the mixed monolayer at lower surface pressures, although this band is not so evident for pure HSt. The band in 1460 cm^{-1} can be attributed to CH_2 deformation and may have its intensity enhanced with OBZ introduction, due to the overlapping of NO_2 stretches in aromatic nitro compounds and also owing to the overlapping of C−O−C vibration in esters, confirming again the presence of OBZ at the interface. The strong negative band in relation to the baseline in 1672 cm^{-1} is attributed to H−O−H bending with strong hydrogen bonding due to water clustering. The negative band is a result of the difference in reflectivity between the interface with and without the coverage of the monolayer.[45] The absence of the band for the mixed monolayer is a clear indication that OBZ affects the hydrating water molecules at the interface.

After transferring the hybrid monolayer to solid supports, the film was characterized with PM-IRRAS in order to confirm the presence of the components on the solid support. The film was then immersed in separated solutions containing PLA2 at different concentrations (c1−c5, with concentration values varying synoptically from 1.0 to 5.0 μg/mL). In Figure 5, the

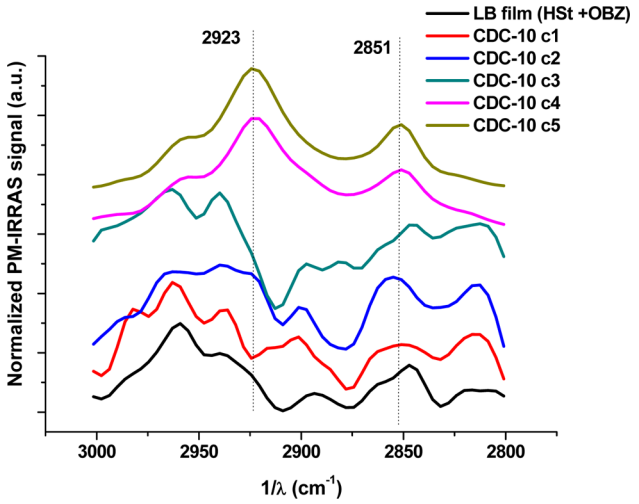

Figure 5. PM-IRRAS spectra for LB film (HSt + OBZ) after in contact with CDC-10 during 5 min in five concentrations (1−5 μg/mL).

bands for symmetric and antisymmetric CH_2 are noticeably changed. The bands are initially ill-defined as a result of the disorder of the OBZ−HSt film in contact with the solid support. On the other hand, the action of CDC-10 in OBZ, which is an enzyme/substrate pair, indirectly affects the fatty acid so that its molecular packing becomes more ordered. It is likely that OBZ/CDC-10 interaction alters their solubility in water and therefore part of their molecules are desorbed from the film.

For the region of 1000−1800 cm^{-1}, shown in Figure 6, the definition of the amide bands are enhanced as a consequence of the enzyme coadsorption. The band in 1652 cm^{-1} is attributed to amide I in α-helix structures, and that one in 1619 cm^{-1} can be ascribed to β-sheet structures. The bands in 1547 and 1561 cm^{-1} are commonly named amide II and are attributed to N−H bending and C−N stretching vibrations. The band in 1742 cm^{-1}, now clearly denoted, is due to C═O stretches in carboxylic acids or esters, being composed therefore of an

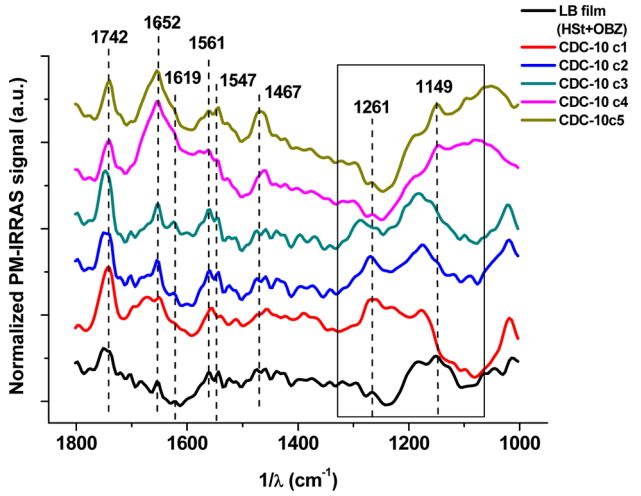

Figure 6. PM-IRRAS spectra for LB film (HSt + OBZ) after in contact with CDC-10 during 5 min in five concentrations (1−5 μg/mL).

overlapping of the bands from HSt and from OBZ. The band that appears at 1467 cm^{-1}, attributed to CH_2 deformation, becomes more intense as long as higher CDC-10 concentrations are inserted in the solution. This vibration is probably from HSt, whose molecular configuration may become more ordered due to substrate desorption. Finally, it is important to note that the bands in 1261 and in 1149 cm^{-1} are markedly affected, which indicated the effect in the vibrations from OBZ, especially for those attributed to ether deformations.

Upon adsorption of carbon nanotubes (CNTs) from its suspension on the hybrid substrate-HSt LB film, changes in the IR spectra can be observed, as shown in Figure 7. The band in

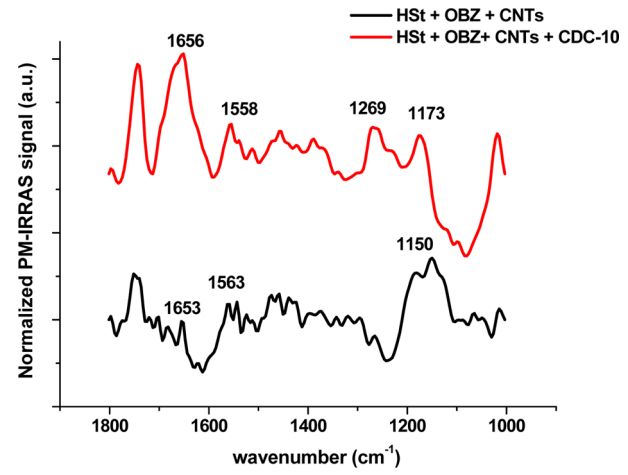

Figure 7. IR spectra for LB film (HSt + OBZ + CNTs) after being in contact with CDC-10 during 5 min in five concentrations (1 μg/mL).

1150 cm^{-1} is related to the ether bending and is slightly shifted in relation to the band found for the film without CNTs. The shoulder in 1184 cm^{-1} is contrasted with that one in 1180 cm^{-1}. The contact with the protein shifted the ether band to 1150 cm^{-1} and enhanced the bands in 1269 cm^{-1} and in the region of 1500−1800 cm^{-1}. These changes confirm that the presence of CNTs may affect the interaction between substrate and CDC-10 and may create a new molecular accommodation for the enzymatic action on the film surface.

dx.doi.org/10.1021/jp307585k | J. Phys. Chem. B 2012, 116, 13424−13429

The enzyme activity of CDC-10 is noticeably preserved in the LB film (activity is kept in about 90% of that one in homogeneous solution), as shown in Figure 8 and detailed in

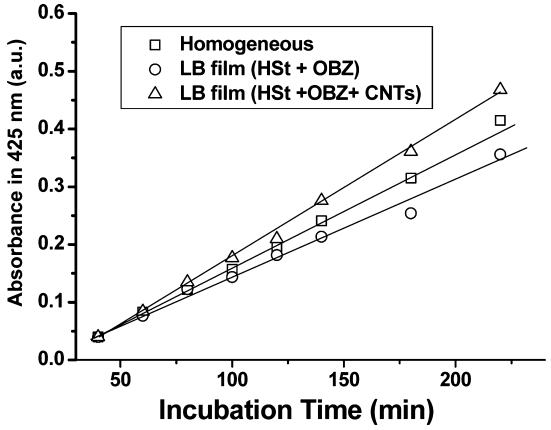

Figure 8. Kinetic plots showing the enzyme action on OBZ for the three systems studied.

Table 1. Mass of Substrate for LB Films Determined via QCM, Enzyme Activity, and Michaelis–Menten Parameters for Homogeneous Solution and Hybrid LB Films

system	mass of substrate (ng)	activity (%)	K_m (10^{-2} mmol L^{-1})
homogeneous	3.50	100	1.52 ± 0.04
LB film (HSt + OBZ)	3.52	91	1.82 ± 0.03
LB film (HSt +OBZ+ CNTs)	3.48	113	1.01 ± 0.02

Table 1, confirming that the highly ordered film helps the enzyme to find a favorable environment for its catalytic action. The environment is apparently enhanced with the presence of CNTs, for which the enzyme-measured activity that was measured is even higher than that one in homogeneous environment. This can be explained by the ordered structure provided by the hybrid CNT-HSt-OBZ film, which facilitates the access of the enzyme onto the solid surface. In this interaction, the phenomena of diffusion, adsorption of the enzyme, and changing of the secondary and tertiary structures of the polypeptide moiety must be involved. It is well-known that enzymes change easily their conformation, which is affected by environmental aspects. As a result, it is likely that the changes observed by PM-IRRAS with the presence of CNTs may facilitate the interaction between the lipid substrate and the catalytic site of the enzyme.

Also, it is important to emphasize that stearic acid was employed to provide an environment that allowed the enzyme substrate (OBZ) to be cospread on the air–water interface and to be further transferred to solid supports as LB films. As a matter of fact, this lipid decreased the PLA2 enzyme activity, as shown in Table 1. The enzyme activity was enhanced only with the incorporation of carbon nanotube. Therefore, this lipid did not serve to improve the enzyme activity, but permitted the construction of hybrid OBZ–carbon nanotube films as systems considered molecularly organized.

Although CNTs could obstruct the interaction between the enzyme in solution and OBZ on the solid support, the catalytic activity increased. This may therefore suggest that OBZ is not completely entrapped between the solid support and CNT layers. Instead, the presence of carbon nanotubes in LB films should provide an architecture that facilitates the exposure of OBZ on the surface for the catalytic sites of the enzyme. Such configuration provides an optimized molecular geometry that causes a more efficient catalysis. Therefore, we should not consider that the carbon nanotubes cover uniformly HST-OBZ LB film, but they must provide an architecture for the efficient contact between the enzyme and its substrate.

The fundamental aspects presented in this paper are important in the sense that information on interactions involving film components could be accessed at the molecular level. Also, one may envisage the employment of CNTs as a suitable scaffold for new hybrid systems capable of preserving the integrity and properties of biomolecules adsorbed on solid matrices.

4. CONCLUSIONS

The high enzyme activity of the hybrid substrate-HSt-CNTs was exploited in a proof-of-concept experiment for the action of CDC-10. Of particular relevance was the possibility to explain why some structure performed better than the other in terms of catalytic activity and permitting the use of carbon nanotubes to enhance the molecular architecture. It is also clear the indication that improved hybrid inorganic–organic bioinspired devices, such as biosensors, can be achieved if fundamental studies on interfaces are carried out. In this context, the incorporation of carbon nanotubes affected the molecular organization of the hybrid lipid ultrathin film and had a fundamental role in the action of the phospholipase present in the external environment. Also, a secondary structure of the enzyme is markedly differentiated when in contact with the film with or without the carbon nanotube.

AUTHOR INFORMATION

Corresponding Author

*E-mail: lcaseli@unifesp.br (L.C.); jr.siqueira@fisica.uftm.edu.br (J.R.S.). Tel.: +55 11 3319-3568 (L.C.); +55 34 3318-5909 (J.R.S.). Fax: +55 11 4043-6428 (L.C.); +55 34 3318 5958 (J.R.S.).

Notes

The authors declare no competing financial interest.

ACKNOWLEDGMENTS

The authors are grateful to CNPq, FAPEMIG, FAPESP (Grant No. 2008/10851-0), and Rede nBionet—Films and Sensors (CAPES, Brazil) for the financial support.

REFERENCES

(1) Cho, M. Y.; Lee, J. M.; Chung, S. J.; Chung, B. H. *Biomaterials* **2009**, *30*, 1197–1204.
(2) Hook, A. L.; Voelcker, N. H.; Thissen, H. *Acta Biomater.* **2009**, *5*, 2350–2370.
(3) Girard-Egrot, A. P.; Godoy, S; Blum, L. J. *Adv. Colloid Interface Sci.* **2005**, *116*, 205–225.
(4) Kini, R. M. *Toxicon* **2003**, *42*, 827–840.
(5) Pinho, F. M. O.; Pereira, I. D. *Rev. Assoc. Med. Bras.* **2001**, *47*, 24–29.
(6) Pirolla, R. A. S.; Baldasso, P. A.; Marangoni, S.; Moran, P. J. S.; Rodrigues, J. A. R. *J. Braz. Chem. Soc.* **2011**, *22*, 300–307.
(7) Selistre de Araújo, H. S.; White, S. P.; Ownby, C. L. *Arch. Biochem. Biophys.* **1996**, *326*, 21–30.

(8) Six, D. A.; Dennis, E. A. *Biochim. Biophys. Acta* **2000**, *1488*, 1−19.
(9) Blodgett, K. B. *J. Am. Chem. Soc.* **1934**, *56*, 495−495.
(10) Zanon, N. C. M.; Oliveira, O. N., Jr.; Caseli, L. *J. Colloid Interface Sci.* **2012**, *373*, 69−74.
(11) Sassolas, A.; Blum, L. J.; Leca-Bouvier, B. D. *Biotechnol. Adv.* **2012**, *30*, 489−511.
(12) Caseli, L.; Siqueira, J. R., Jr. *Langmuir* **2012**, *28*, 5398−5403.
(13) Qi, Y. B. *Surf. Sci. Rep.* **2011**, *66*, 379−393.
(14) Heath, J. R. *Ann. Rev. Mater. Res.* **2009**, *39*, 1−23.
(15) Ceridório, L. F.; Balogh, D. T.; Caseli, L. *J. Colloid Interface Sci.* **2010**, *346*, 87−95.
(16) Schmidt, T. F.; Caseli, L.; Viitala, T.; Oliveira, O. N., Jr. *Biochim. Biophys. Acta, Biomembr.* **2008**, *1778*, 2291−2297.
(17) Iost, R. M.; Madurro, J. M.; Brito-Madurro, A. G.; Nantes, I. L.; Caseli, L.; Crespilho, F. N. *Int. J. Electrochem. Sci.* **2011**, *5*, 1085−1104.
(18) Pavinatto, F. J.; Fernandes, E. G. R.; Alessio, P.; Constantino, C. J. L.; de Saja, J. A.; Zucolotto, V.; Apetrei, C.; Oliveira, O. N., Jr.; Rodriguez-Mendez, M. L. *J. Mater. Chem.* **2011**, *13*, 4995−5003.
(19) Caseli, L.; Nobre, T. M.; Silva, D. A. K.; Loh, W.; Zaniquelli, M. E. D. *Colloids Surf., B* **2001**, *22*, 309−321.
(20) Rosetti, C. M.; Maggio, B.; Oliveira, R. G. *Biochim. Biophys. Acta* **2008**, *1778*, 1665−1675.
(21) Maget-Dana, R. *Biochim. Biophys. Acta* **1999**, *1462*, 109−140.
(22) Xianming, K.; Xuezhong, D. *J. Phys. Chem. B* **2011**, *115*, 13191−13198.
(23) Ariga, K.; Nakanishi, T.; Hill, J. P. *Soft Matter* **2006**, *2*, 465−477.
(24) Garima, T.; Miodrag, M.; Leblanc, R. M. *Colloids Surf., B* **2009**, *74*, 436−456.
(25) Siqueira, J. R., Jr.; Gasparotto, L. H. S.; Oliveira, O. N., Jr.; Zucolotto, V. *J. Phys. Chem. C* **2008**, *112*, 9050−9055.
(26) Siqueira, J. R., Jr.; Abouzar, M. H.; Poghossian, A.; Zucolotto, V.; Oliveira, O. N., Jr.; Schöning, M. J. *Biosens. Bioelectron.* **2009**, *25*, 497−501.
(27) Siqueira, J. R., Jr.; Werner, C. F.; Bäcker, M.; Poghossian, A.; Zucolotto, V.; Oliveira, O. N., Jr.; Schöning, M. J. *J. Phys. Chem. C* **2009**, *113*, 14765−14770.
(28) Siqueira, J. R., Jr.; Bäcker, M.; Poghossian, A.; Zucolotto, V.; Oliveira, O. N., Jr.; Schöning, M. J. *Phys. Status Solidi A* **2010**, *207*, 781−786.
(29) Siqueira, J. R., Jr.; Maki, R. M.; Paulovich, F. V.; Werner, C. F.; Poghossian, A.; de Oliveira, M. C. F.; Zucolotto, V.; Oliveira, O. N., Jr.; Schöning, M. J. *Anal. Chem.* **2010**, *82*, 61−65.
(30) Sousa Luz, R. A.; Martins, M. V. A.; Magalhães, J. L.; Siqueira, J. R., Jr.; Zucolotto, V.; Oliveira, O. N., Jr.; Crespilho, F. N.; Silva, W. C. *Mater. Chem. Phys.* **2011**, *130*, 1072−1077.
(31) Katz, E.; Willner, I. *ChemPhysChem* **2004**, *5*, 1085−1104.
(32) Kim, S. N.; Rusling, J. F.; Papadimitrakopoulos, F. *Adv. Mater.* **2007**, *19*, 3214−3228.
(33) Kim, J.; Lee, S. W.; Hammond, P. T.; Shao-Horn, Y. *Chem. Mater.* **2009**, *21*, 2993−3001.
(34) Lee, S. W.; Kim, B. S.; Chen, S.; Shao-Horn, Y.; Hammond, P. T. *J. Am. Chem. Soc.* **2009**, *131*, 671−679.
(35) Itamar Willner, I.; Willner, B. *Nano Lett.* **2010**, *10*, 3805−3815.
(36) Siqueira, J. R., Jr.; Caseli, L.; Crespilho, F. N.; Zucolotto, V.; Oliveira, O. N., Jr. *Biosens. Bioelectron.* **2010**, *25*, 1254−1263.
(37) Lee, S. W.; Kim, J.; Chen, S.; Hammond, P. T.; Shao-Horn, Y. *ACS Nano* **2010**, *4*, 3889−3896.
(38) Romero-Vargas, F. F.; Ponce-Soto, L. A.; Martins-de-Souza, D.; Marangoni, S. *Comp. Biochem. Physiol. C* **2010**, *151*, 66−74.
(39) Cho, W.; Kézdy, F. J. *Methods Enzymol.* **1991**, *197*, 75−79.
(40) Holzer, M.; Mackessy, S. P. *Toxicon* **1996**, *34*, 1149−1155.
(41) Beghini, D. G.; Toyama, M. H.; Hyslop, S.; Sodek, L. C.; Novello, J. C.; Marangoni, S. J. *Protein Chem.* **2000**, *19*, 679−684.
(42) Davies, J. T.; Rideal, E. K. *Interfacial Phenomena*; Academic Press: New York, 1963.
(43) Hayashi, S.; Umemura, J. *J. Chem. Phys.* **1975**, *63*, 1732−1740.
(44) Umemura, J. *J. Chem. Phys.* **1978**, *68*, 42−46.
(45) Blaudez, D.; Boucher, F.; Buffeteau, T.; Desbat, B.; Grandbois, M.; Salesse, C. *Appl. Spectrosc.* **1999**, *53*, 1299−1304.